Available online at www.sciencedirect.com
ScienceDirect
Geochimica et Cosmochimica Acta 70 (2006) 4130–4139
Geochimica
www.elsevier.com/locate/gca

The behavior of trace elements during schwertmannite precipitation and subsequent transformation into goethite and jarosite

Patricia Acero [a,*], Carlos Ayora [a], Clara Torrentó [a], José-Miguel Nieto [b]

[a] *Earth Sciences Institute Jaume Almera, CSIC, Barcelona, Spain*
[b] *Geology Department, University of Huelva, Huelva, Spain*

Received 6 February 2006; accepted in revised form 15 June 2006

Abstract

Schwertmannite is a ubiquitous mineral formed from acid rock drainage (ARD), and plays a major role in controlling the water chemistry of many acid streams. The formation of schwertmannite was investigated in the acid discharge of the Monte Romero abandoned mine (Iberian Pyrite Belt, SW, Spain). Schwertmannite precipitated from supersaturated solutions mainly owing to the oxidation of Fe(II) to Fe(III) and transformed with time into goethite and jarosite. In a few hours, schwertmannite precipitation removed more than half of the arsenic load from solution, whereas the concentration of divalent trace metals (Zn, Cu, Pb, Cd, Ni, and Co) remained almost unchanged. In the laboratory, natural schwertmannite was kept in contact with its coexisting acid water in a flask with a solid–liquid mass ratio of 1:5 for 353 days. During this time, the pH of the solution dropped from 3.07 to 1.74 and the concentrations of sulfate and Fe increased. During the first 164 days, schwertmannite transformed into goethite plus H_3O-jarosite but, subsequently, goethite was the only mineral to form. Some of the trace elements, such as Al, Cu, Pb, and As were depleted in solution during the first stage as schwertmannite transformed into goethite plus H_3O-jarosite. On the contrary, the transformation of schwertmannite to goethite (with no jarosite) during the second stage released Al, Cu, and As to the solution. Despite the variation in their concentrations in solution, approximately 80% of the total Al and Cu inventories and more than 99% As and Pb remained in the solid phase throughout the entire aging process.

1. Introduction

The behavior of trace elements in acid rock drainage (ARD) is controlled by several factors, such as mineralogy of the primary ores and enclosing rocks, weathering conditions and hydrological variability. Moreover, newly formed precipitates from ARD, such as jarosite, schwertmannite, and goethite may play a key role in the removal of trace elements from solution (Bigham et al., 1994; Webster et al., 1998).

Schwertmannite is a Fe(III)-oxyhydroysulfate that forms commonly in waters with pH values between 3.0 and 4.5 and sulfate concentrations between 1000 and 3000 mg L^{-1} (Bigham et al., 1994). It has been recognized in many ARD streams (Bigham et al., 1994, 1996; Yu et al., 1999); in the waters and sediments of lakes receiving ARD (Schwertmann et al., 1995; Childs et al., 1998; Regenspurg et al., 2004) and in the substrates of wetlands treating ARD (Gagliano et al., 2004). Schwertmannite has been reported to remove arsenic from waters in acid streams (Courtin-Nomade et al., 2003; Fukushi et al., 2003) and in mine tailings (Dold and Fontbote, 2002).

Schwertmannite is a metastable phase, and has been found to transform into goethite over timescales of weeks to months. During their laboratory experiment, Bigham et al. (1996) placed a synthetic specimen of schwertmannite in contact with distilled water and observed that it transformed into goethite over a period of 543 days, releasing sulfate, Fe and H^+ to the solution. The reaction proposed for the transformation by these authors was

* Corresponding author. Fax: +34 93 4010012.
E-mail address: pacero@ija.csic.es (P. Acero).

0016-7037/$ - see front matter © 2006 Elsevier Inc. All rights reserved.
doi:10.1016/j.gca.2006.06.1367

$$Fe_8O_8(OH)_{5.5}(SO_4)_{1.25}(s) + 2.5H_2O = 8FeOOH(s) + 1.25SO_4^{2-} + 2.5H^+ \quad (1)$$

Other experimental studies on synthetic schwertmannite found that the rate of the transformation into goethite was slower for high sulfate concentrations, low pH and low temperature (Jönsson et al., 2005). High amounts of As in synthetic schwertmannite have also been shown to retard or inhibit the transformation into goethite (Fukushi et al., 2003; Regenspurg and Peiffer, 2005). The transformation of schwertmannite into goethite has also been suggested to occur in natural environments. For instance, Gagliano et al. (2004) found that schwertmannite had transformed at depth into goethite, in vertical sediment profiles of a constructed mine drainage wetland.

For schwertmannite to be considered an efficient trace element sink, elements removed from solution must be retained in the solid phase throughout its transformation into other mineral phases. However, the question of how schwertmannite recrystalization into goethite (reaction 1) affects the trapped elements still remains unclear. It is reasonable to assume that the more crystallized a mineral is (goethite compared with schwertmannite), the less it can include trace elements in its structure or sorbed on the surface. At field scale, one of the few evidences of trace element behavior is based on the comparison between extracts in ammonium oxalate of schwertmannite and goethite samples from a waste-rock pile (Schroth and Parnell, 2005). In that study, schwertmannite was collected from the bed of an active acid stream whereas goethite was found above the water table, and was assumed to have formed from prior schwertmannite. They showed that the amount of trace elements retained in the solid phase throughout the transformation is variable, and proposed a qualitative retention scale: Pb > Zn, Mn > As, Al, and Cu. However, other experiments of leaching with precipitates from ARD do not show As remobilization during in situ transformation of schwertmannite into goethite (Courtin-Nomade et al., 2005), and demonstrate that the process is not entirely understood.

The present work is focused on the transformation of natural schwertmannite into more stable phases with aging and on the behavior of the trace elements in this transformation. Two types of study have been carried out; (1) a comparison between field samples of fresh and aged precipitates in an acid stream, and (2) a laboratory experiment consisting in aging monominerallic natural schwertmannite under controlled conditions.

2. Materials and methods

2.1. Field site and sampling description

All the samples of water and precipitates used in this study were collected from the acid discharge of the abandoned Monte Romero mine (Iberian Pyrite Belt, SW, Spain), which mined a massive pyrite deposit enriched with copper and zinc. The acid stream flows from a pool fed by underground galleries. Four sampling points (CM1 to CM4) were set up along a 40 m reach before the stream enters an underground intake. The water flow varies seasonally, and ranges from an average of 3.5 L s^{-1} in winter (rainy) to 1.5 L s^{-1} in summer (dry). In the rainy season, however, the excess of water flows directly from CM1 to the intake, ensuring a continuous flow of about 1.5 L s^{-1} from sampling point CM1 (pool) to CM4.

The stream bed is made up of low permeability schist and is covered with several centimeters of brownish, crusty precipitates, creating different terrace levels along the channel. The volume of water contained in the terraces between point CM1 and CM4 is 15 m^3, and the residence time of water was estimated to be approximately 2.8 h under the average flow conditions ($Q = 1.5$ L s^{-1}). No other water inflows were detected in the stream reach under study.

At each sampling point (CM1 to CM4), pH, Eh, temperature, and electrical conductivity were measured and two water samples were taken in acid-pre-washed polyethylene bottles, after rinsing thoroughly with the local water. One of the water samples was filtered at 0.45 μm and acidified with 1 mL of concentrated HNO_3 for each 50 mL of solution, for major cation, sulfur and trace element analysis. The other water sample was filtered at 0.1 μm and acidified with HCl, adjusting its pH to less than 1 for Fe(II)/Fe(III) determination. Blank and duplicate samples were also taken during the sampling campaigns for quality assurance purposes. All the samples were preserved at 4 °C until analyses.

Solid samples of precipitates were also taken from the surface of the stream bed and at different depths down to 20 cm at all the sampling points. The samples were dried at room temperature for mineralogical determination.

2.2. Analytical methods

A pH-meter and combined electrode with temperature compensation was used to measure pH and was calibrated regularly in the laboratory and in the field with standard buffer solutions of pH 2, 4, and 7. Eh was measured using a Pt combination electrode that was calibrated with standard buffer solutions of 220 and 468 mV. Measurements were corrected to the Standard Hydrogen Electrode. Electrical conductivity was performed with a Pt cell calibrated with KCl 0.1 and 0.01 m solutions. The measurement errors for pH, Eh, and conductivity were $\leqslant$0.02 pH units, $\leqslant$5 mV and $\pm$1%, respectively.

The concentrations of Fe, Cu, Zn, Na, Al, Ca, Mg, and S in solution were measured by inductively coupled plasma atomic emission spectrometry (ICP-AES) using a Thermo Jarrel-Ash instrument with CID detector. Detection limits were 10 μg l^{-1} for Fe, Cu, and Zn, 100 μg l^{-1} for Na and 50 μg l^{-1} for Al, Ca, Mg, and S and the error was estimated to be below 3%. The concentrations of As, V, Sr, Cd, Pb, Ni, and Co were determined by inductively coupled plasma atomic mass spectroscopy (ICP-MS) using a X-series II

Thermo instrument. Detection limits were in the order of 1 μg l^{-1} and the error was estimated to be below 5%. In the analyses of ICP-AES and ICP-MS, calibration with sets of standards was performed and the regression coefficients exceeded 0.999. Three laboratory standards were analyzed with every 10 samples to check for accuracy. In the analyses of ICP-AES and ICP-MS, dilutions from 1:2 to 1:100 were performed to ensure that the concentration of the samples was within the concentration range of the standards.

Ferrous and total dissolved iron concentrations (following reduction with hydroxylamine hydrochloride) were determined by colorimetry using the ferrozine method (modified after To et al., 1999) in a UV–VIS HP Spectrophotometer within one month of field sampling. Fe(III) was taken as the difference between Fe(tot) and Fe(II). The quality of the results was assured by measuring several standards, blanks and duplicates. In addition, Fe(tot) concentrations matched ICP-AES results within 5%. This consistency suggests that no significant amount of iron particles passed through the 0.45 μm filter.

The chemical composition of the precipitates was determined by analysis of the leachate obtained in total acid digestion according to the method developed by Querol et al. (1996).

X-ray diffraction (XRD) of powdered samples was used in an attempt to identify the minerals present in each precipitate sample using a Bruker D5005 difractometer with Cu Kα radiation. Powdered samples were scanned from 0° to 60° 2θ with a continuous scan at a rate of 0.025°/18 s.

Selected Au coated samples of precipitates were observed under field-emission scanning electron microscopy (SEM) using an Hitachi H-4100FE with intensity current between 15 and 20 kV to ascertain whether the changes in the mineralogy of precipitates were associated with major variations in morphology and surface appearance. The specific surface area of the solid samples was determined by the BET-method (Brunauer et al., 1938) with a Micromeritics ASAP 2000 using 5 point N_2-adsorption isotherms.

2.3. Aging experiment

In January 2004, one sample of approximately 200 g of fresh ochreous precipitate was collected at the sampling point CM3, together with the coexisting acid water for the aging experiment. The sample of fresh schwertmannite was kept in contact with a similar volume of acid water (about 1 L in total) in a polyethylene bottle to reproduce pore water conditions under controlled laboratory conditions. No quantitative solid:liquid ratio was measured at this stage in order to prevent the perturbation of the natural sample. Both solid and coexisting water were kept at room temperature (22 ± 3 °C), and in the presence of light for 353 days. In order to allow contact with atmospheric oxygen without evaporative water losses, the lid of the polyethylene bottle was microdrilled.

The system was stirred on a regular basis and small volumes of water (8 mL) were collected every 6–20 days for hydrochemical analysis, pH and temperature determination. A solid sample of about 1 g was also taken every month, rinsed with ethanol, dried at room temperature, weighed, and then stored for XRD and SEM characterization. At the end of the experiment, a small fraction of the solid sample was digested to obtain the bulk chemical composition (Table 1, sample 2). From the weight of the solid and liquid that remained at the end of the experiment, and considering the quantities of solid and liquid collected periodically, the initial solid and liquid masses were estimated to be 201 and 915 g, respectively. This corresponds to an initial solid:liquid weight ratio of 0.22, which remained consistent throughout the experiment.

3. Results and discussion

3.1. Schwertmannite precipitation at the Monte Romero site

Samples of precipitates were taken from the surface of the acid stream bed and from depths of up to 20 cm at the four sampling points. Surface samples consisted of a yellow-orange powder and a highly porous and brittle brown solid. The samples gained stiffness and a dark brown coloration with depth. Examination of powdered solid samples with XRD revealed that all the fresh surface precipitates corresponded to monominerallic schwertmannite, whereas goethite and jarosite were the only phases detected in the sub-surface precipitates. The inspection of the samples under SEM showed different crystal morphology between surface and sub-surface samples. The typical schwertmannite aggregates of spheres with pin-cushion morphology were observed in the fresh surface precipitates, whereas the deeper samples showed similar spherulitic aggregates but made up of elongated and planar crystals. As discussed below, very similar morphologies were observed in the solid phase at the beginning and at the end of the aging experiments, respectively.

Table 1
Major constituents (wt %) of (1) monominerallic schwertmannite precipitate from Monte Romero (sample CM3-January 2004), and (2) the same sample after 353 days of aging

Sample	Mineral	Al_2O_3	As_2O_5	Fe_2O_3	ZnO	CaO	MgO	CuO	PbO	K_2O	Na_2O	SO_3	H_2O^*
(1)	Sch	0.45	0.56	54.38	0.19	0.14	0.17	0.02	0.02	0.04	0.03	12.50	22.73
(2)	Gt + Jt	0.47	0.63	59.57	0.23	0.13	0.17	0.01	0.02	0.05	0.04	8.29	11.57

Sch = schwertmannite; Gt = goethite; Jt = H_3O-jarosite; H_2O^* = water content below 105 °C. The structural water above 105 °C and organic matter constituents were not analyzed.

Table 2
Chemical characteristics of Monte Romero AMD waters during three sampling campaigns at the four sampling points

	Sample (filtered)	T (°C)	pH	Eh (mV)	Cond (μS cm^{-1})	mg L^{-1}									μg l^{-1}							
						SO_4	Fe_{tot}	Fe(II)	Ca	Mg	Na	K	Al	Zn	Cu	Sr	Cd	Pb	Ni	Co	As	V
February 2003	CM-1	20.1	2.92	—	4698	3697	402	246	212	237	19	1	147	495	17	204	792	84	1044	764	467	22
	CM-2	18.0	2.65	—	4713	3724	382	215	214	238	19	1	147	504	18	198	752	79	946	768	346	15
	CM-3	16.2	3.03	—	4633	3642	386	205	209	234	19	1	145	490	17	185	714	91	744	734	265	12
	CM-4	15.7	3.00	—	4604	3641	363	175	209	234	19	1	145	495	17	189	748	101	876	724	219	11
June 2003	CM-1	23.0	3.24	535	4629	3784	318	254	212	265	20	2	137	434	12	18	88	24	790	840	152	2
	CM-2	23.0	3.20	599	4540	3766	320	216	208	265	20	2	137	435	12	19	84	20	400	840	55	2
	CM-3	23.8	2.82	688	4810	3958	256	160	217	278	21	2	145	459	13	20	87	26	260	900	22	1
	CM-4	25.2	2.64	705	5084	4056	234	140	227	288	21	1	150	473	13	22	98	27	400	900	24	1
January 2004	CM-1	19.0	3.27	581	3922	3095	320	245	185	218	19	1	132	383	12	241	787	96	838	605	562	17
	CM-2	18.3	3.17	617	4045	3194	313	230	192	228	19	1	135	398	13	245	849	92	895	670	453	15
	CM-3	15.9	3.07	637	3968	3143	284	181	189	224	19	1	133	393	13	221	779	92	815	582	348	9
	CM-4	15.4	2.82	633	3946	3077	265	152	186	221	19	1	131	386	12	232	786	95	781	568	283	9

From the analyses of the leachate obtained in total acid digestion of the precipitate sample taken at point CM3 in January 2004 (Table 1, sample 1) the stoichiometry of the Monte Romero schwertmannite was deduced to be $Fe_8O_8(OH)_{4.32}(SO_4)_{1.84}$:n$H_2O$. The sulfate value is higher than the one proposed by Bigham et al. (1996) but within the range of 1.74–1.86 suggested by Yu et al. (1999). The purity of the sample was proved by XRD, and the chemical analysis is given in Table 1 (sample 1).

The field parameters and water analyses from the four sampling points of the acid stream for three sampling campaigns are shown in Table 2. Differences in temperature between winter and summer were always less than 5 °C. Major element-chemistry was very similar in the different sampling campaigns and corresponded to sulfate-rich water with high Zn, Fe, and Al contents.

The saturation state of the water analyses with respect to schwertmannite were calculated using the code PHREEQC (Parkhusrt, 1995) and the WATEQ4F database (Ball and Nordstrom, 1991). As shown in Fig. 1, if the solubility product proposed by Bigham et al. (1996) is assumed ($\log K = 18 \pm 2.5$), some of our samples seem to be subsaturated with respect to schwertmannite, which is inconsistent with the field evidence of precipitation. This observed supersaturation suggests the value of 10.5 ± 2 proposed by Yu et al. (1999) may be more appropriate in this case. This feature has also been observed for analyses of water coexisting with schwertmannite from other studies (e.g., Fukushi et al., 2003; Regenspurg et al., 2004).

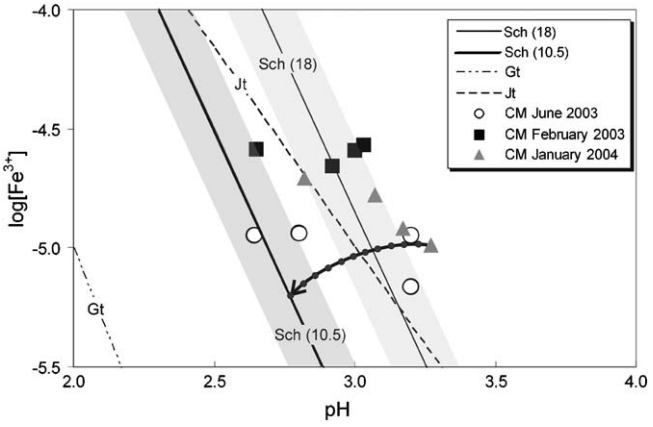

Fig. 1. Log Fe^{3+} activity vs. pH plots of the analyses of water coexisting with schwertmannite in the samples from the Monte Romero acid drainage. The lines represent the equilibrium of different iron phases: Jt = H_3O-jarosite, Gt = goethite (WATEQ4F database, Ball and Nordstrom, 1991), Sch(18) = schwertmannite (Bigham et al., 1996), Sch(10.5) = schwertmannite (Yu et al., 1999). The grey-shaded areas show solubility windows for both $\log K_{sp}$ values (±2.5). Solubility curves are calculated assuming an activity of SO_4^{2-} of $10^{-2.7}$mol L^{-1}. The arrow indicates the trend calculated for schwertmannite precipitation in a closed system. The arrow has been calculated by removing small amounts of schwertmannite from the CM1 (January 04) solution, and performing successive speciation calculations with the PHREEQC code.

The solution supersaturation and the process leading to schwertmannite precipitation can be explained by the hydrogeochemical data. As seen in Table 2, pH decreased downstream from sampling point CM1 to CM4 in the two last sampling campaigns. Both ferrous and total iron concentrations decreased systematically downstream (Table 2), indicating that Fe(II) was oxidized to Fe(III), which was removed from the solution by the precipitation of schwertmannite. Fe^{3+} activity in solution remained constant or slightly increased along the sampled reach (Fig. 1) in contrast to the expected decrease associated to schwertmannite precipitation in a closed system (showed by the arrow in Fig. 1). This suggests that the oxidation of Fe(II) is faster than the schwertmannite precipitation. Thus, the kinetics of the overall process was deduced to be controlled by the precipitation of schwertmannite.

The evolution of trace element concentrations downstream showed two contrasting patterns. On one hand, Zn, Cu, Cd, Pb, and Co did not experience any significant change, and Ni showed only a slight decrease downstream. On the other hand, the concentrations of As and V showed a systematic decrease downstream in all the sampling campaigns. The variations in the behavior of these trace elements can be attributed to the different affinity of each aqueous species to the schwertmannite surface. According to WATEQ4F (Ball and Nordstrom, 1991) and MINTEQA2 (Allison et al., 1990) databases, at pH 3 and for the observed sulfate concentration in the stream, the predominant aqueous species for divalent metals is the uncharged complex MSO_4^0 (M = Co, Ni, Cd, Pb, and Zn), whereas main aqueous species for As and V are anions, ($H_2AsO_4^-$ and $VO_2SO_4^-$). Since, schwertmannite has a point of zero charge of 7.2 (Jönsson et al., 2005) its surface is positively charged at acid pH, and only As and V species are therefore expected to be sorbed onto the schwertmannite surface.

3.2. Schwertmannite aging experiment

3.2.1. Evolution of precipitates

The mineralogical evolution of the solid samples during the aging experiment can be observed in Fig. 2. The presence of goethite is confirmed by XRD 105 days after the start of the experiment. After 148 days of experiment, the presence of goethite and jarosite is evident in the XRD spectrum. Finally, schwertmannite peaks are almost entirely absent in the XRD spectrum after 323 days. This mineralogical evolution corresponds to a change in the morphology of the precipitates. Thus, the typical pin-cushion shape of schwertmannite switches to a morphology in which the sphericity of the aggregates is preserved but the individual crystals are less rounded and more planar (see Fig. 3).

No distinction among different jarosite forms was possible from the XRD spectra. Mass-balance calculations suggest that H_3O-jarosite is the mineral present in our system. Thus, the existence of the calculated proportion (see below)

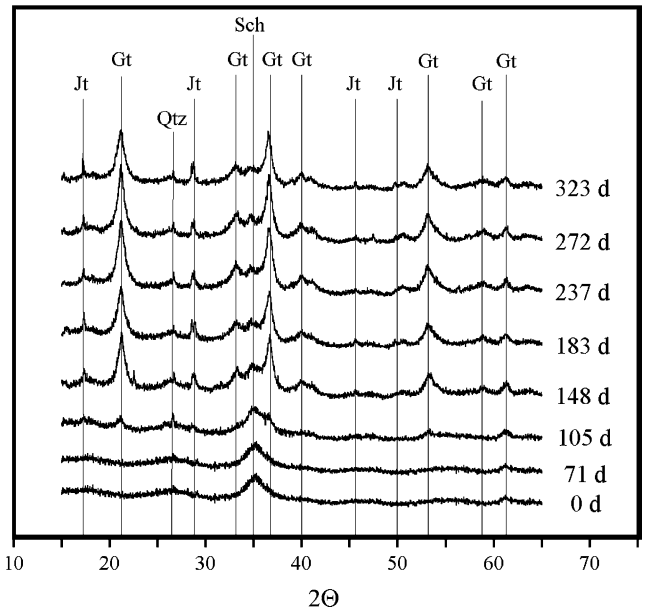

Fig. 2. X-ray diffraction patterns for samples taken at different times (in days) during the laboratory experiment on schwertmannite aging. Sch: schwertmannite; Gt: goethite; Jt: jarosite. The diagrams show the evolution from pure schwertmannite (0 day) to goethite plus jarosite (323 days).

of jarosite as K-jarosite or Na-jarosite would require up to 3 and 2 wt% K_2O and Na_2O in the analysis of the solid remaining after the experiment (Table 1). Likewise, the formation of these minerals would have led to a significant decrease in K and Na concentration in aqueous solution, which was not recorded (Table 3).

The BET surface area of the initial schwertmannite was 80 ($\pm$8) $m^2\,g^{-1}$, somewhat less than the range of 100–300 $m^2\,g^{-1}$ previously specified for the mineral (Bigham et al., 1990; Cornell and Schwertmann, 1996). Closer to the values recorded here, Webster et al. (1998) and Jönsson et al. (2005) reported surface areas of 55 $m^2\,g^{-1}$ and 42.9 $m^2\,g^{-1}$, respectively. According to the literature, the transformation from schwertmannite to a more crystalline mineral involves particle growth and an increase in density from 3.75–3.90 $g\,cm^{-3}$ of schwertmannite (Bigham et al., 1990) to 4.26 $g\,cm^{-3}$ of goethite (Cornell and Schwertmann, 1996). This process may cause a decrease in surface area. However, during the laboratory aging experiment, the surface area of the solid was not recorded to change substantially (from 80 ± 8 to 84 ± 8 $m^2\,g^{-1}$).

3.2.2. Evolution of major elements in solution

The chemical evolution of the solution during the aging experiment can be observed in Table 3. Thus, pH in the water decreased throughout the experiment from 3.07 to 1.74, whereas iron and sulfate concentrations increased from 284 to 5545 mg L^{-1} and from 3143 to 18421 mg L^{-1}, respectively. Fe(II) was assumed to oxidize to Fe(III) after a few days in contact with the atmosphere, in agreement

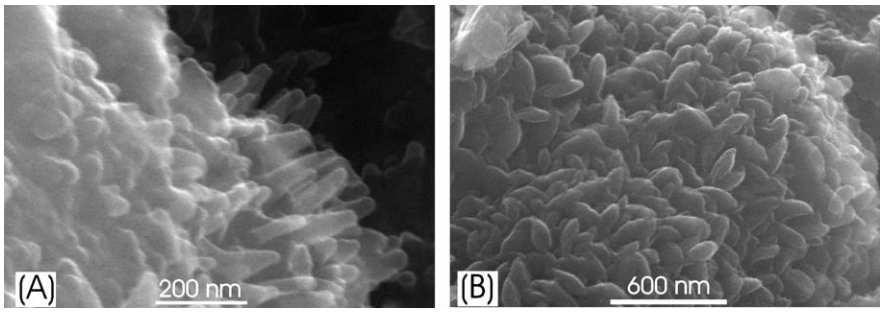

Fig. 3. Field emission scanning electron microscopy images of the solids: (A) at the beginning (schwertmannite), and (B) at the end (goethite + jarosite) of the laboratory experiment on schwertmannite aging.

Table 3
Evolution of the mineralogy of the solid phase, and of major and trace elements in solution of the schwertmannite aging laboratory experiment

Time (days)	Minerals	pH	(mg L^{-1})								$\mu g\ L^{-1}$					S.I.				
			Fe	Cu	Zn	Na	Al	Ca	Mg	SO_4	As	Ni	Co	Cd	Pb	Sch (10.5)	Sch (18.0)	Gt	Jt	Jb
0	Sch	3.07	284	13	393	19	133	189	224	3143	350	815	580	780	90	13.3	5.8	5.9	3.4	0.6
71	Sch	2.75	1057	11	442	24	100	200	254	4668	20	1100	670	905	185	11.4	3.9	5.5	3.5	0.1
77		2.65	792	12	450	23	100	200	261	4542	b.d.	870	680	870	210	8.5	1.0	5.1	2.7	0.0
90		2.61	1385	9	446	24	54	203	266	5563	b.d.	680	660	920	180	9.4	1.9	5.2	3.2	−0.3
97		2.71	2756	5	423	23	23	199	254	7514	b.d.	860	720	895	145	n.c.	n.c.	n.c.	n.c.	n.c.
105	Sch, (Gt)	2.60	3494	4	439	24	11	211	270	9020	b.d.	990	740	895	105	11.5	4.0	5.4	4.1	−1.1
118		2.56	3458	3	401	23	7	202	256	9239	b.d.	900	740	845	60	10.8	3.3	5.3	3.9	−1.3
132		2.55	4187	3	387	23	13	203	254	10593	b.d.	1190	750	860	55	11.0	3.5	5.3	4.0	−1.0
148	Sch, Gt, Jt	2.42	4744	3	370	23	36	206	259	11864	5	1080	690	870	50	9.2	1.7	5.1	3.7	−0.7
164		2.39	5445	4	388	25	77	220	273	13955	15	900	700	940	30	8.8	1.3	5.0	3.7	−0.4
183	Gt, Jt, (Sch)	2.27	5444	6	379	24	131	213	264	14964	150	890	750	910	25	6.5	−1.0	4.6	3.1	−0.3
199		2.17	5422	6	377	23	152	212	264	15752	440	870	740	795	10	4.5	−3.0	4.3	2.6	−0.4
220		2.00	5527	7	381	23	157	217	870	16765	740	870	790	930	15	1.1	−6.4	3.8	1.8	−0.5
237	Gt, Jt, (Sch)	1.84	5572	6	376	18	160	213	266	17184	790	650	720	870	15	−2.0	−9.5	3.4	1.1	−0.7
255		1.87	5561	8	371	29	165	177	213	17027	770	n.a.	n.a.	705	50	−1.4	−8.9	3.5	1.2	−0.6
272	Gt, Jt, (Sch)	1.78	5657	8	391	21	177	185	226	17931	875	n.a.	n.a.	740	10	−3.3	−10.8	3.2	0.8	−0.7
296		1.79	5677	8	383	23	171	188	220	17457	685	n.a.	n.a.	700	30	−2.9	−10.4	3.2	0.9	−0.7
323	Gt, Jt	1.93	5198	9	412	20	189	193	238	18374	565	n.a.	n.a.	880	15	−1.3	−8.8	3.5	1.3	−0.5
353	Gt, Jt	1.74	5545	9	434	20	199	203	251	18421	600	n.a.	n.a.	790	10	−4.6	−12.1	3.0	0.5	−0.7

Potassium was always below 1 mg L^{-1}. Sch = schwertmannite, Gt: goethite; Jt: H_3O-jarosite; Jb = jurbanite; b.d.: below detection limit; n.a.: not analysed; S.I.: saturation index; n.c.: no convergence of the speciation code is achieved. S.I. calculations made with the code PHREEQC, and the WATEQ4F database, with the exception of Sch(10.5) (Yu et al., 1999) and Sch(18.0) (Bigham et al., 1996).

with published field oxidation rates (Noike et al., 1983; Nordstrom, 1985; Kirby and Elder-Brady, 1998), and with the Fe(II) decrease observed from CM1 to CM4 after 2.8 h of residence time (Table 2). Indeed, some analyses performed during the aging experiment confirmed that the Fe(II) proportion was always below 10%. Therefore, in the speciation calculations we assumed that all the Fe analyzed was Fe(III).

Considering the evolution of the solution composition in more detail, two periods can be distinguished (Fig. 4). During the first 164 days, both sulfate and iron concentrations increased at a constant molar ratio of 1.14 (Fig. 5). Then (from 164 to 237 days), increasing sulfate and constant iron concentrations were clearly observed (Fig. 5). After this date, no significant changes in the iron and sulfate concentrations or in pH were observed. Taking into account the observed evolution of the solid phases and of the coexisting solutions, these two periods can be interpreted in the following way:

(1) From 0 to 164 days: transformation of schwertmannite into H_3O-jarosite and goethite according to the overall reactions

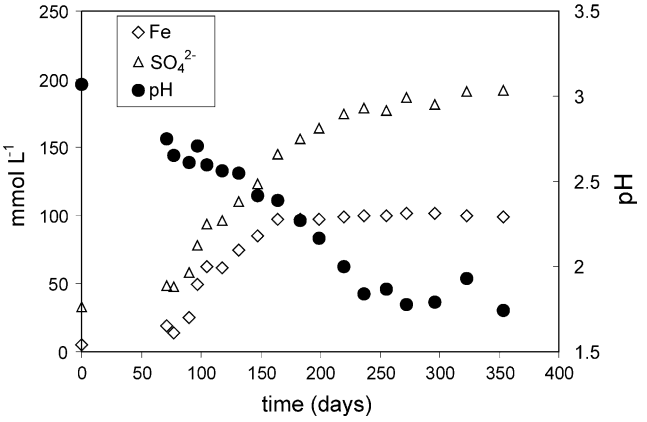

Fig. 4. Evolution of pH, sulfate and Fe concentration in the aqueous solution from the schwertmannite aging experiment.

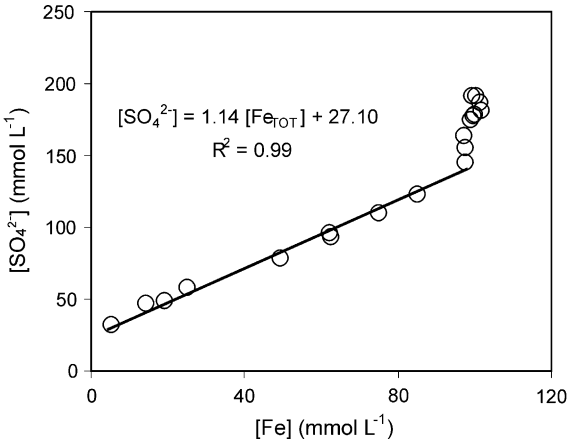

Fig. 5. Evolution of the SO_4:Fe experimental ratio of the aqueous solution in the schwertmannite aging experiment.

$$x_1Fe_8O_8(OH)_{4.32}(SO_4)_{1.84}(s) + u_1H_2O \rightarrow z_1(H_3O)Fe_3(SO_4)_2(OH)_6(s) + r_1SO_4^{2-} + q_1Fe^{3+} + p_1H^+ \quad (2)$$

$$y_1Fe_8O_8(OH)_{4.32}(SO_4)_{1.84}(s) + 3.68y_1H_2O \rightarrow 8y_1FeOOH(s) + 1.84y_1SO_4^{2-} + 3.68y_1H^+ \quad (3)$$

(2) From 164 to 237 days: transformation of schwertmannite into goethite according to the overall reaction

$$y_2Fe_8O_8(OH)_{4.32}(SO_4)_{1.84}(s) + 3.68y_2H_2O \rightarrow 8y_2FeOOH(s) + 1.84y_2SO_4^{2-} + 3.68y_2H^+ \quad (4)$$

The stoichiometric coefficients in the reactions (2) to (4) can be calculated from the variation in the measured concentrations and from mass balance constraints, according to the criteria described in Table 4. The results, normalized to 1 L solution, for the first period of the experiment are:

$$0.047Fe_8O_8(OH)_{4.32}(SO_4)_{1.84}(s) + 0.068H_2O + 0.098SO_4^{2-} + 0.494H^+ \rightarrow 0.092(H_3O)Fe_3(SO_4)_2(OH)_6(s) + 0.099Fe^{3+} \quad (5)$$

Table 4
Relationships among the stoichiometric coefficients of reactions (2) to (4) of transformation of schwertmannite into goethite and jarosite

$r_1 + 1.84y_1 = \alpha$	$\alpha = [SO_4]_{(t\ =\ 164\ \text{days})} - [SO_4]_{(t\ =\ 0)} = 0.1126$
$1.84y_2 = \beta$	$\beta = [SO_4]_{(t\ =\ 353\ \text{days})} - [SO_4]_{(t\ =\ 164)} = 0.0465$
$q_1 = (r_1 + 1.84y_1)/\varepsilon$	ε = [SO4]:[Fe] from day 0 to 164 = 1.14 (Fig. 5)
$8x_1 = 3z_1 + q_1$	Fe mass balance
$1.84x_1 = 2z_1 + r_1$	Sulfate mass balance
$12.32x_1 + u_i = 7z_1$	Oxygen mass balance (except oxygen in sulfate)
$4.32x_1 + 2u_1 = 9z_1 + p_1$	Hydrogen mass balance
$8(x_1 + y_1 + y_2) = \delta$	Mol of Fe in initial solid phase (220 g); $\delta = (WS)/(Mv) = 1.496$

All the calculations are normalised to 1 L of solution and the concentrations of iron and sulfate are expressed in mol L^{-1}. Legend: W = wt% of Fe_2O_3 in the solid analysis (Table 1, sample 1), S = solid/liquid ratio (estimated of 220 g L^{-1}), M = Mol weight of Fe_2O_3, v = stoichiometric coefficient of iron in Fe_2O_3.

$$0.115Fe_8O_8(OH)_{4.32}(SO_4)_{1.84}(s) + 0.416H_2O \rightarrow 0.917FeOOH(s) + 0.211SO_4^{2-} + 0.422H^+ \quad (6)$$

And for the second period

$$0.025Fe_8O_8(OH)_{4.32}(SO_4)_{1.84}(s) + 0.093H_2O \rightarrow 0.202FeOOH(s) + 0.047SO_4^{2-} + 0.093H^+ \quad (7)$$

The calculation of the pH evolution requires the speciation of the solution. To this end, the processes represented by (5) to (7) were simulated according to the reaction progress equations:

$$\frac{dc_i}{dt} = A \cdot s \cdot R_{sh}(0.162v_{i,sh} - 0.917v_{i,gt} - 0.092v_{i,jt}) \quad c_i^0 = c_i(0\ \text{days}) \quad (8)$$

$$\frac{dc_i}{dt} = A \cdot s \cdot R_{sh}(0.025v_{i,sh} - 0.202v_{i,gt}) \quad c_i^0 = c_i(164\ \text{days}) \quad (9)$$

where c_i is the concentration of the i solute (mol L^{-1}), C_i^0 is the initial concentration, A is the specific surface (80 $m^2\ g^{-1}$), s is the solid/liquid ratio (220 g L^{-1}), $v_{i,m}$ is the stoichiometric coefficient of the solute i in the mineral m (where schwertmannite is sh, goethite is gt, and jarosite is jt) and R_{sh} is the transformation rate of schwertmannite (mol $m^{-2}\ s^{-1}$). The calculations were performed with the reactive transport code RETRASO (Saaltink et al., 2004), using the WATEQ4F thermodynamic database (Ball and Nordstrom, 1991). For simplicity, A, s, and R_{sh} were assumed to be constant throughout the process. A value of 6×10^{-10} mol $m^{-2}\ s^{-1}$ for R_{sh} was obtained by fitting the calculated and experimental values of iron concentrations. This value is a first approximation since it is expected to vary with saturation. The values of SO_4 and pH calculated with the reaction progress described by Eqs. (8) and (9) were also checked with the experimental values. As shown in Fig. 6, the calculated evolution of pH versus SO_4 matches the experimental values reasonably well (±0.2), demonstrating the suitability of the proposed model.

Finally, as an independent test, the jarosite:goethite molar fraction deduced from reactions (5) to (7) is 0.082, which is similar to 0.086, the value that is obtained from the bulk analysis of the solid residual after the experiment (Table 1, sample 2) if all the analyzed sulfur in the solid is assumed to form H_3O-jarosite.

As shown above, two parallel reactions of schwertmannite to jarosite and schwertmannite to goethite explain the change in the solution chemistry and in the precipitate mineralogy. The kinetics of these two reactions seems to be controlled by supersaturation, as suggested by the trends of the saturation indexes shown in Table 3. Thus, the solution was initially supersaturated with respect to goethite and jarosite, and both minerals precipitated. As the reactions progressed, the solution approached equilibrium with jarosite, and the formation of this mineral almost ceased. On the contrary, the solution remains supersaturated with respect to goethite until the end of the experiment.

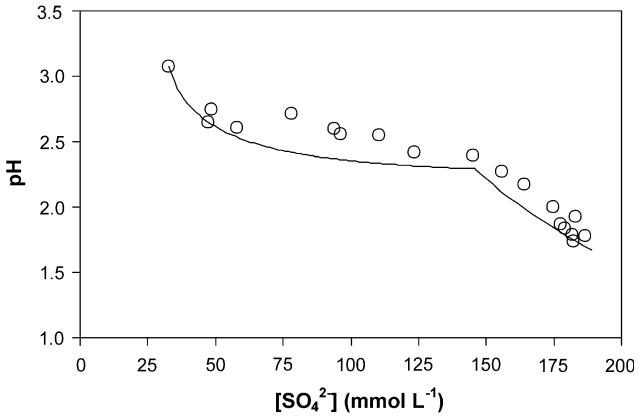

Fig. 6. Evolution of the SO_4:pH ratio of the aqueous solution in the schwertmannite aging experiment. Circles = experimental data; line = calculated.

This evolution is qualitatively similar to the results presented by Bigham et al. (1996). Nevertheless, the evolution observed in our experiments is faster than the rates documented by these authors. The fact that in our experiments the transformation was almost complete after only 353 days (vs. 543 days in the work by Bigham et al., 1996) can be due to the use in our study of a lower initial pH and a higher solid:solution ratio. Another interesting difference is that, whereas in the experiment of Bigham et al. (1996) all the schwertmannite transformed into goethite, the presence of jarosite has been unambiguously detected in our experiments. This difference can be attributed to the much higher sulfate concentration in our experiments (always >30 mmol L^{-1} vs. a maximum of 2 mmol L^{-1} in Bigham et al., 1996).

The other major elements in solution are Na, Ca, Mg, and Zn. Their concentrations remained almost unchanged during the experiment (Table 3), indicating the lack of reaction with the solid Fe–S–O phases involved in the system. This also suggests that evaporation was negligible during the aging experiment.

However, Al underwent an interesting evolution, first decreasing from 133 to 7 mg L^{-1} and then increasing to 199 mg L^{-1}. The minimum recorded concentration coincided with the first sampling in which goethite peaks became evident in the XRD patterns of the solid sample. It is difficult to attribute the evolution of Al concentration to sorption/desorption processes on the surface of the iron phases, since the aqueous speciation of Al does not significantly change within the measured pH range; $AlSO_4^+$, $Al(SO_4)_2^-$ and Al^{3+} being the predominant species. The evolution of Al concentrations may be attributed to the precipitation of jurbanite ($AlOHSO_4$) during the first part of the experiment and the latter dissolution of this mineral. This hypothesis is supported by the calculated saturation states of the solution with respect to jurbanite (Table 3). Alternatively, the Al decrease coincides with the formation of H_3O-jarosite indicating that Al could be co-precipitated with this mineral. Indeed, Al currently replaces Fe(III) in the jarosite structure, giving rise to the jarosite-alunite series (Dutrizac and Jambor, 2000). The later increase in Al concentration could be attributed to the lack of jarosite precipitation but with part of the schwertmannite still dissolving.

3.2.3. Evolution of trace elements in solution

Although present in lower concentrations, the evolution of dissolved Cu is the same as described for Al. Cu has also been reported to incorporate in minor amounts in minerals of the jarosite group (Scott, 1987).

As in the case of Zn, the concentrations of trace cations such as Ni, Co, and Cd did not show any significant change throughout the aging process (Table 3), suggesting that they were not incorporated in the goethite or jarosite structures. Under our experimental conditions all these elements form an uncharged aqueous complex species with sulfate, MSO_4^0, which must have also avoided adsorption on the positively charged surfaces of the Fe–S–O phases.

In the case of Pb, its concentration initially increased sharply from 90 to 210 μg L^{-1} and then dropped progressively to values close to 10 μg L^{-1} (Table 3). The initial increase may be related to desorption due to the decrease of pH during the early part of the experiment. The subsequent decrease in the Pb concentrations may be attributed to adsorption on goethite surface and co-precipitation in the jarosite structure. Spectroscopic studies (IR, XAFS) have demonstrated that Pb-SO_4 ternary complexes form on the goethite surface, enhancing the Pb adsorption, mainly at low pH and high sulfate concentrations (Weesner and Bleam, 1998; Elzinga et al., 2001). By contrast, Pb has been reported to occupy the structural sites of K, Na, and H in jarosite, becoming a major constituent in plumbojarosite (Dutrizac and Jambor, 2000). The most significant decrease in Pb concentration took place during the first part of the aging experiment together with the formation of H_3O-jarosite, suggesting a major role of H_3O-jarosite in Pb retention.

The most relevant evolution, however, is shown by As, which decreased from 350 μg L^{-1} to below the detection limit, and then increased again to 600 μg L^{-1} towards the end of the experiment. The As removal coincides with schwertmannite presence (first 34 days) and H_3O-jarosite formation (first 164 days). By contrast, As increased in solution when goethite was the only solid to form (after day 164), suggesting that goethite is a less efficient As sink than schwertmannite and jarosite. In the literature, the ability of schwertmannite to immobilize As has been previously reported (Dold and Fontbote, 2002; Courtin-Nomade et al., 2003; Fukushi et al., 2003). However, the relative ability of jarosite and goethite to retain As remains unclear. Whereas some earlier studies claim that As can remain immobilized in jarosite by replacing sulfur in sulfate tetrahedra (Savage et al., 2000, 2005), other works show that As is retained preferentially in goethite over jarosite (Strawn et al., 2002). Another possible explanation for

the As release in the last part of the aging experiment is the switch of As(V) aqueous speciation from $H_2ASO_4^-$ to $HAsO_4^0$ predominance at pH around 2.5 (Dixit and Hering, 2003), which could contribute to the As desorption as pH decreases. Unfortunately, the lack of data on As sorption on goethite at pH lower than 4 makes it impossible to explore this possibility further at present, although it should certainly be addressed in the future.

Despite the variation in their concentrations in solution, about 80% of the total Al and Cu inventories and more than 99% As and Pb remained in the solid phase throughout the entire aging process.

Acknowledgments

We acknowledge J. Elvira, M. Cabañas, and R. Bartrolí (Institute of Earth Sciences Jaume Almera, CSIC) for assistance in XRD and chemical analysis. SEM observations were carried out at the Serveis Cientific-Tècnics of the University of Barcelona with the advice of J. Garcia-Veigas. We also acknowledge George Von Knorring and Will Mayes for improving the English style of this paper. The comments and suggestions of the associate editor and three anonymous reviewers significantly improved the original manuscript. This work was funded by the Spanish MEC project REN-2003-09590.

Associate editor: George R. Helz

References

Allison, J.D., Brown, D.S., Novo-Gradac, K.L., 1990. MINTEQA2/PRODEFA2, A Geochemical Assessment Model for Environmental Systems, Version 3.0 User's Manual. Environmental Research Laboratory, Office of Research and Development, U.S. EPA, Athens, GA.

Ball, J., Nordstrom, D., 1991. User's manual for WATEQ4F with revised thermodynamic database and test cases for calculating speciation of major, trace and redox elements in natural waters. U.S. Geological Survey Water-Resources Investigation Report 91–183.

Bigham, J.M., Schwertmann, U., Carlson, L., Murad, E., 1990. A poorly crystallized oxyhydroxisulfate of iron formed by bacterial oxidation of Fe(II) in acid-mine waters. *Geochim. Cosmochim. Acta* **54** (10), 2743–2758.

Bigham, J.M., Carlson, L., Murad, E., 1994. Schwertmannite, a new iron oxyhydroxysulphate from Pyhasalmi, Finland, and other localities. *Mineral. Mag.* **58** (393), 641–648.

Bigham, J.M., Schwertmann, U., Traina, S.J., Winland, R.L., Wolf, M., 1996. Schwertmannite and the chemical modeling of iron in acid sulfate waters. *Geochim. Cosmochim. Acta* **60** (12), 2111–2121.

Brunauer, S., Emmet, P., Teller, E., 1938. Adsorption of gases in multimolecular layers. *J. Am. Chem. Soc.* **60**, 309–319.

Childs, C.W., Inoue, K., Mizota, C., 1998. Natural and anthropogenic schwertmannites from Towada-Hachimantai National Park, Honshu, Japan. *Chem. Geol.* **144** (1-2), 81–86.

Cornell, R., Schwertmann, U., 1996. *The iron oxides*. VCH, Weinheim.

Courtin-Nomade, A., Bril, H., Neel, C., Lenain, J.F., 2003. Arsenic in iron cements developed within tailings of a former metalliferous mine, Enguiales, Aveyron, France. *Appl. Geochem.* **18** (3), 395–408.

Courtin-Nomade, A., Grosbois, C., Bril, H., Roussel, C., 2005. Spatial variability of arsenic in some iron-rich deposits generated by acid mine drainage. *Appl. Geochem.* **20** (2), 383–396.

Dixit, S., Hering, J.G., 2003. Comparison of arsenic(V) and arsenic(III) sorption onto iron oxide minerals: implications for arsenic mobility. *Environ. Sci. Technol.* **37** (18), 4182–4189.

Dold, B., Fontbote, L., 2002. A mineralogical and geochemical study of element mobility in sulfide mine tailings of Fe oxide Cu-Au deposits from the Punta del Cobre belt, Northern Chile. *Chem. Geol.* **189** (3-4), 135–163.

Dutrizac, J., Jambor, J., 2000. Jarosites and their application to hydrometallurgy. In: Alpers, C.N., Jambor, J.L., Nordstrom, D.K. (Eds.), *Sulfate Minerals: Crystallography, geochemistry and environmental significance. Reviews in Mineralogy and Geochemistry*, vol. 40. Mineralogical Society of America, Washington, DC, pp. 405–452.

Elzinga, E.J., Peak, D., Sparks, D.L., 2001. Spectroscopic studies of Pb(II)-sulfate interactions at the goethite–water interface. *Geochim. Cosmochim. Acta* **65** (14), 2219–2230.

Fukushi, K., Sasaki, M., Sato, T., Yanase, N., Amano, H., Ikeda, H., 2003. A natural attenuation of arsenic in drainage from an abandoned arsenic mine dump. *Appl. Geochem.* **18** (8), 1267–1278.

Gagliano, W.B., Brill, M.R., Bigham, J.M., Jones, F.S., Traina, S.J., 2004. Chemistry and mineralogy of ochreous sediments in a constructed mine drainage wetland. *Geochim. Cosmochim. Acta* **68** (9), 2119–2128.

Jönsson, J., Persson, P., Sjoberg, S., Lovgren, L., 2005. Schwertmannite precipitated from acid mine drainage: phase transformation, sulphate release and surface properties. *Appl. Geochem.* **20** (1), 179–191.

Kirby, C.S., Elder-Brady, J.A., 1998. Field determination of Fe^{2+} oxidation rates in acid mine drainage using a continuously-stirred tank reactor. *Appl. Geochem.* **13** (4), 509–520.

Noike, T., Nakamura, K., Matsumoto, J.I., 1983. Oxidation of ferrous iron by acidophilic iron-oxidizing bacteria from a stream receiving acid-mine drainage. *Water Res.* **17** (1), 21–27.

Nordstrom, D., 1985. The rate of ferrous iron oxidation in a stream receiving acid mine effluent. Selected Papers in Hydrogeologic Sciences. U.S.G.S. Water Supply Paper 2270. pp. 113–119.

Parkhusrt, D., 1995. User's guide to PHREEQC: A computer program for speciation, reaction path, advective-transport, and inverse geochemical calculations. U.S. Geological Survey Water-Resources Investigation Report 95–4227.

Querol, X., Alastuey, A., Lopez-Soler, A., Mantilla, E., Plana, F., 1996. Mineral composition of atmospheric particulates around a large coal-fired power station. *Atmos. Environ.* **30** (21), 3557–3572.

Regenspurg, S., Peiffer, S., 2005. Arsenate and chromate incorporation in schwertmannite. *Appl. Geochem.* **20** (6), 1226–1239.

Regenspurg, S., Brand, A., Peiffer, S., 2004. Formation and stability of schwertmannite in acidic mining lakes. *Geochim. Cosmochim. Acta* **68** (6), 1185–1197.

Saaltink, M., Batlle, F., Ayora, C.J.C., Olivella, S., 2004. RETRASO, a code for modelling reactive transport in saturated and unsaturated porous media. *Geol. Acta* **2** (3), 235–251.

Savage, K.S., Tingle, T.N., O'Day, P.A., Waychunas, G.A., Bird, D.K., 2000. Arsenic speciation in pyrite and secondary weathering phases, Mother Lode Gold District, Tuolumne County, California. *Appl. Geochem.* **15** (8), 1219–1244.

Savage, K.S., Bird, D.K., O'Day, P.A., 2005. Arsenic speciation in synthetic jarosite. *Chem. Geol.* **215** (1-4), 473–498.

Schroth, A.W., Parnell, R.A., 2005. Trace metal retention through the schwertmannite to goethite transformation as observed in a field setting, Alta Mine, MT. *Appl. Geochem.* **20** (5), 907–917.

Schwertmann, U., Bigham, J.M., Murad, E., 1995. The 1st occurrence of schwertmannite in a natural stream environment. *Eur. J. Mineral.* **7** (3), 547–552.

Scott, K.M., 1987. Solid-solution in, and classification of, gossan-derived members of the alunite-jarosite family, Northwest Queensland, Australia. *Am. Mineral.* **72** (1–2), 178–187.

Strawn, D., Doner, H., Zavarin, M., McHugo, S., 2002. Microscale investigation into the geochemistry of arsenic, selenium, and iron in

soil developed in pyritic shale materials. *Geoderma* **108** (3-4), 237–257.

To, T., Nordstrom, D., Cunningham, K., Ball, J., McCleskey, R., 1999. New method for the direct determination of dissolved Fe(III) concentration in acid mine waters. *Environ. Sci. Technol.* **33** (5), 807–813.

Webster, J.G., Swedlund, P.J., Webster, K.S., 1998. Trace metal adsorption onto an acid mine drainage iron(III) oxy hydroxy sulfate. *Environ. Sci. Technol.* **32** (10), 1361–1368.

Weesner, F.J., Bleam, W.F., 1998. Binding characteristics of Pb^{2+} on anion-modified and pristine hydrous oxide surfaces studied by electrophoretic mobility and X-ray absorption spectroscopy. *J. Colloid Interface Sci.* **205** (2), 380–389.

Yu, J.Y., Heo, B., Choi, I.K., Cho, J.P., Chang, H.W., 1999. Apparent solubilities of schwertmannite and ferrihydrite in natural stream waters polluted by mine drainage. *Geochim. Cosmochim. Acta* **63** (19–20), 3407–3416.